Investigating Impact of Trapped Charges on Severity of Very Fast Transient Over-Voltages (VFTOs) in a 550kV GIS by modelling Disconnector Switch

*Payal Pramanik[1], M. Gopichand Naik[2]
Research Scholar[1], Professor[2]
[1,2]*Department of Electrical Engineering, Andhra University, Visakhapatnam, INDIA.*

Abstract: *Very Fast Transient Overvoltages (VFTOs) in Gas-Insulated Switchgear (GIS) pose significant challenges to insulation integrity and system reliability, particularly during switching operations. This study investigates the mechanisms contributing to VFTO generation, emphasizing the modeling of the disconnector switch and the influence of trapped charge voltage (TCV) in a 550 kV GIS system. Utilizing EMTP-ATP software, we employed a multi-spark approach to model the disconnector switch and examined VFTO characteristics under various TCV conditions. Key parameters such as rise time, peak time, and overshoot factors were meticulously simulated and analyzed to quantify the severity of transient overvoltages. The results indicate that increased TCV levels considerably elevate VFTO magnitudes and peak response times; for instance, simulations showed a rise time increase up to 1.18 times and a peak overshoot factor that exceeded 30 kV/ns under extreme TCV conditions. Furthermore, the simulated results highlighted the impact of trapped charges on the severity of VFTOs especially while working with EHV/UHV GIS where the ratio of lightening impulse withstand voltage (LIWV) to VFTO gets lowered. These insights not only deepen our understanding of VFTO behavior in GIS systems but also inform strategies for supressing trapped charge accumulation on the surface of GIS equipment.*

Keywords: **Gas-Insulated Switchgear (GIS), Very Fast Transient Overvoltages (VFTOs), Disconnector Switch (DS), Trapped Charge Voltage (TCV), EMTP-ATP.**

1. INTRODUCTION

Gas-Insulated Substations (GIS) are high-voltage substations used extensively for connecting transmission networks to generation stations and distribution systems [1]. As a compact, reliable, and low-maintenance alternative to Air-Insulated Substations, GIS enclosures integrate all essential control and protection switchgear within sealed compartments, utilizing sulfur hexafluoride (SF6) gas as an insulating medium. With the surge in urbanization and advances in ultra-high voltage transmission, GIS technology has gained global prominence due to its superior insulation, operational reliability, and enhanced safety features [2,3&4].

Despite these advantages, GIS systems face challenges from overvoltages, which are categorized by IEC standards into temporary and transient types. Transient overvoltages are further divided into slow-front, fast-front, and very-fast-front transients, with Very Fast Transient Overvoltages (VFTOs) presenting a significant risk to GIS integrity [5]. VFTOs, triggered primarily during switching operations within GIS or through vacuum circuit breakers in medium-voltage networks, pose potential threats by causing internal flashovers and high-touch voltages [6 and 7]. Specifically, the pre-striking of GIS disconnectors or re-ignition of SF6 circuit breakers generates very fast transient fronts that demand careful analysis and mitigation.

VFTOs can be classified into internal and external types based on the stress points within GIS systems. Internal VFTOs arise between the inner conductor and enclosure, while external VFTOs impact neighboring equipment, potentially reaching the Basic Impulse Level (BIL) of connected transformer windings and requiring various mitigation measures

[7]. Past studies have proposed multiple techniques for VFTO mitigation within GIS, including frequency spectrum analysis for accurate VFTO measurement in 220/66kV GIS units [8]. Furthermore, advancements in disconnector switch operations have highlighted the role of multi-spark phenomena in arc ignition and extinction, opening avenues for improved VFTO management strategies [9].

To address these VFTO challenges, several studies have introduced reactive power compensation and proposed novel damping techniques, such as using nanocrystalline ferrite rings to mitigate high-frequency oscillations caused by VFTOs [10-12]. Additionally, methodologies for accurate VFTO measurement have been developed to analyze amplitude and spark associations, and experimental studies have explored factors influencing VFTOs, such as GIS height, pipe length, and soil resistivity, to better understand their impact on insulation reliability [13]. Capturing the intricate nature of Very Fast Transient Overvoltages (VFTOs) in Gas-Insulated Switchgear (GIS) requires sophisticated modeling approaches, especially for elements like the disconnector switch, which generates transient overvoltages due to rapid switching [14]. Developing accurate multi-spark models and simulating transient conditions are technically challenging, particularly in terms of replicating real-world conditions in software like EMTP-ATP [15 and 16]. Quantifying the effects of TCV variations on VFTO characteristics is critical but challenging due to the non-linear interactions within the GIS system [17 and 18]. Variations in TCV can lead to vastly different transient behaviors, making it essential to thoroughly investigate a range of TCV scenarios to understand their impact on overvoltage peaks and insulation stress.

While previous studies recognize TCV as a factor in VFTO generation, there is a lack of in-depth quantitative analysis on how varying levels of TCV specifically influence rise times, peak overshoot, and overall VFTO magnitude [19 and 20]. This gap restricts comprehensive understanding, especially when designing insulation that can withstand different VFTO levels. Current literature has explored VFTO modeling, but detailed methods for accurately simulating the disconnector switch with multi-spark behavior remain underrepresented [21]. Incorporating such techniques could improve predictive capabilities for VFTOs generated under realistic GIS operating conditions [22-24]. Many studies have not fully explored the implications of VFTO severity on GIS insulation and system reliability across varied TCV levels [25]. Addressing this gap is critical to improving GIS design, making it more resilient to extreme transient events.

The major contributions in this paper are:

1. This study presents a novel approach to modeling the disconnector switch in GIS using a multi-spark framework. By accurately simulating multiple switching events, the model gives in-depth knowledge on constraints involved in real time designing of disconnector switch.
2. Through a comprehensive set of simulations, this study quantifies the effects of TCV on key VFTO parameters such as rise time, peak time, and overshoot factors. Results indicate that higher TCV levels significantly amplify VFTO magnitudes, with rise times increasing by up to 1.12-1.18 times and overshoot factors exceeding 30 kV/ns under extreme conditions.
3. By addressing the impact of VFTOs under varied TCV scenarios, the findings contribute valuable data to decide future insulation standards, aiming to suppress surface charges and mitigate VFTO effects and enhance GIS reliability in high-voltage applications.

This paper presents a simulation and analysis of VFTOs generated by disconnector switch operations, examining their effects on GIS insulation reliability. A multi-spark model, based on breakdown voltages across gaps, is employed to simulate the opening and closing dynamics of the disconnector switch under various trapped charge voltages, using EMTP-ATP software to model a 550 kV GIS system. The results focus on key VFTO characteristics, including overshoot factor, rise-time, and peak-time, and provide valuable information on various factors that are responsible to pose challenges in operation and control of Gas Insulated switchgear.

The remainder of this paper is structured as follows: Section 2 details the critical parameters for modeling disconnector switch arcing. Section 3 presents the design and simulation of the 550kV GIS in ATP-Draw. Section 4 describes multi-spark approach for closing operation of Disconnector switch in EMTP-ATP. Sections 5 and 6 summarize the simulation results and evaluate VFTO characteristics, respectively. Section 7 presents the graphical analyzation of parameters involved in determining VFTO severity. Section 8 gives summary on strategies involved to suppress trapped charges followed by conclusion in Section 9.

2. CONSIDERATIONS FOR DISCONNECTOR MODELLING

When modelling the disconnector contact operation, understanding parameters such as breakdown voltage, arc ignition and extinction time, arc and contact gap resistance, and trapped charge is essential for accurately simulating VFTOs. This section provides an overview of these critical factors that influence VFTO generation.

2.1. Breakdown characteristics

Breakdown voltage, the minimum voltage at which an electrical insulator fails, is a crucial parameter in GIS design. It is generally a linear function of the contact gap distance, which varies over time. Two methods for determining the Breakdown Voltage (BDV) of a GIS disconnector are commonly used for multi-spark analysis: a theoretical approach that derives a linear voltage curve from disconnector nameplate data, and a practical approach involving field-test measurements [15].
The BDV for the opening and closing operations can be calculated using the following formulae [15].

For opening operation: $U_{BDV}^{op+/-}(t) = \frac{+/-U_W}{t_{op}}(t - t_0^{op})$ (1)

For closing operation: $U_{BDV}^{cl+/-}(t) = U_W - \frac{+/-U_W}{t_{cl}}(t - t_0^{cl})$ (2)

where U_W is the withstand voltage across the disconnector switch (a standard value specified in the equipment nameplate), $U_{BDV}^{op}(t)$ or $U_{BDV}^{cl}(t)$ represent the breakdown voltages for opening and closing operations, t_0^{op} or t_0^{cl} are the initiation times for opening and closing, and t_{op} or t_{cl} denote the operation intervals provided by the manufacturer.

2.2. Spark arc duration

When the voltage across the disconnector exceeds withstand threshold, flashover occurs, creating a conductive arc path across the gap. This breakdown time t_B is typically a few nanoseconds and results in a rapid transition in gap resistance from maximum to minimum. The spark arc duration, generally estimated between 2 and 20 nanoseconds, can be calculated using the Toepler equation as outlined in [15]. Once the spark is initiated, it sustains the current until it falls below 1 A. Assuming an initial current of 10 kA, the extinguishing time can be estimated using an exponential decay function, typically ranging between 50 and 100 microseconds.

For modeling disconnector contacts, spark resistance is critical. Spark resistance has two main components: arc resistance and gap resistance. Arc resistance is often assumed to be a constant value of 0.5 ohms [19], while gap resistance during transitions (opening to closing and vice versa) can be calculated using the Toepler equation which is given by [15].

$$t_B = 13.3\frac{k_T}{E_O.\eta.p} \quad (3)$$

k_T is the Toepler coefficient for SF_6 gas
E_O is the dielectric field strength for SF_6 gas and is approximated to be 860 kV/cm/MPa.
η is the Utilization factor of electric filed and is assumed as 0.7.
p is the pressure of SF_6 gas which is approximately 0.45 MPa.

The resistance expressions for ignition and extinction are given by [15]:

$$R_{ig}^{n}(t) = R_{arc} + (R_{gap} - R_{arc})e^{\frac{-(t-t_s^n)}{\tau}} \quad (4)$$

and

$$R_{ex}^{n}(t) = R_{arc} + (R_{gap} - R_{arc}).(1 - e^{-t\frac{[t-(t_s^n-\Delta t_s^n)]}{\tau}}) \quad (5)$$

R_{arc} is the resistance of arc, R_{gap} is the contact gap resistance.
t_s^n is the time instant of n[th] spark ignition.
Δt_s^n is the time duration of the n[th] spark.
τ is the total time constant which can be estimated as 0.67ns from Toepler equation.

[17] reveals the estimated trapped charge (TC) levels with varying breakdown symmetry (5%, 15%, 30%) and arcing time of 0.6 seconds, as shown in Figure 1.

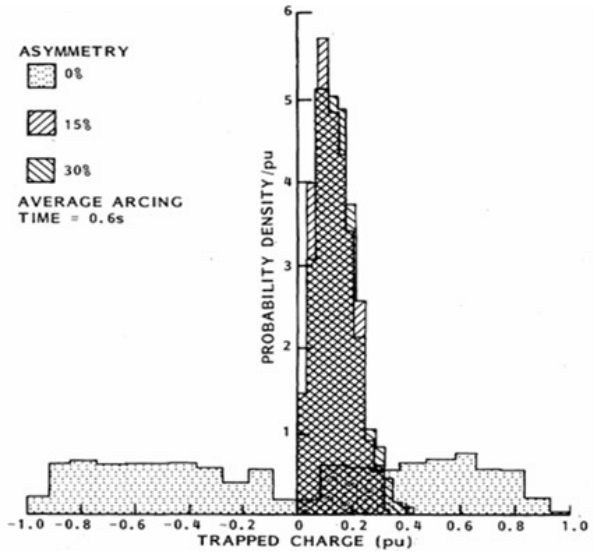

Figure 1. Probable amount of TC with Variable BD Symmetry

2.3. Trapped Charge

The design and behavior of trapped charges play a pivotal role in disconnector switch modeling. Trapped charges, generated at the load side of the disconnector when the switch operates, decay gradually and significantly influence breakdown voltage levels during re-closing. A high trapped charge increases the probability of breakdown at elevated voltages upon re-closing, potentially causing conductor-to-ground overvoltages. Research [17] demonstrates that a trapped charge of 1 p.u. results in an initial breakdown at 2 p.u. across the switch contacts, potentially causing conductor-to-ground overvoltages of up to 2.5 p.u. Field studies at Ontario Hydro's Clareville substation (550 kV GIS) [17] further show that residual trapped charges on the unconnected disconnector side are generally between 0.1 and 0.2 p.u., underscoring the role of trapped charge in VFTO generation.

3. MODELLING OF GIS SWITCHGEAR

The simulation of 550kV GIS done in this paper is taken from past literature [19] where the plant in Northern Brazil had failure at CB-2 and DS-4 of phase B of bay 2. The point of failure (node N_1 and node N_2) was monitored for over voltages using EMTP-ATP software for various TCVs to analyze the severity of VFTOs which is very critical while working with EHV/UHV transmission systems.

3.1. Disconnector switch modelling

The primary objective of modeling the disconnector switch is to monitor Very Fast Transient Overvoltages (VFTOs) generated during switching operations. This paper presents the design of a disconnector switch capable of producing multi-spark events, modeled using the EMTP-ATP Draw software.

The key design concept involves comparing the voltage across the disconnector switch with the breakdown potential of the contact gap to determine if an arc should ignite or extinguish. Figure 2 [19] illustrates the modeling of a time-dependent TACS (Transient Analysis of Control Systems) resistor, which depends on voltage inputs from both the source and load sides of the disconnector, as well as on capacitive current.

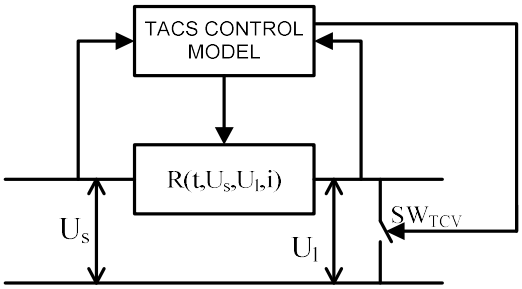

Figure 2. TACS Control Module with Various Inputs and Outputs.

The control technique involved in developing the TACS module in order to operate the disconnector switch is described in the flowchart given in Figure. 3

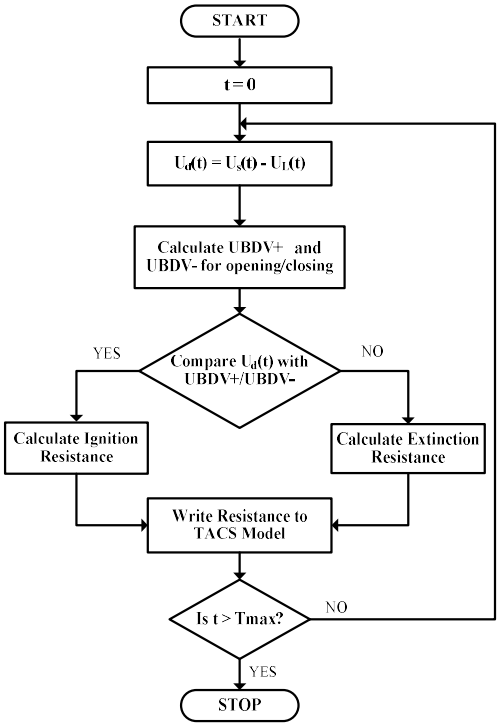

Figure 3. Flowchart for opening/closing of DS using multi-spark approach

For switch movement, two operating speeds are considered:

1. Manual operation at 0.15 m/s (crank-operated)
2. Motorized operation at 1.5 m/s

The remainder of the GIS system is modeled using a distributed parameter approach [19]. The GIS system includes two generators (G_A and G_B) with ratings of 390 MVA and 13.8 kV, and two transformers (T_A and T_B) rated at 405 MVA with a voltage ratio of 13.8/550 kV, connecting to a 550 kV GIS network. A single-line diagram (SLD) of the 550 kV GIS system is provided below.

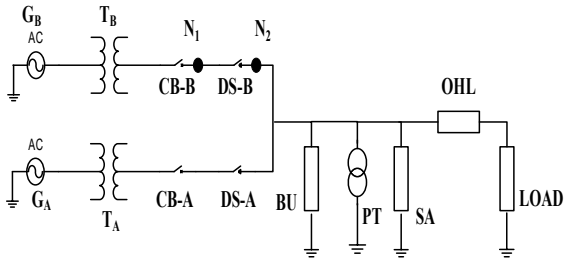

Figure 4. Simplified Single Line Diagram (SLD) of the 550 kV GIS showing damaged nodes N_1 and N_2.

In Figure 4, a simplified busbar configuration for the 550 kV GIS is shown, displaying only two circuit breakers and disconnector switches to reduce complexity. Generally, the simulation model includes four disconnector switches (DS-A, DS-B, DS-C, and DS-D) and two circuit breakers (CB-A and CB-B). DS-A and DS-C isolate CB-A, while DS-B and DS-D isolate CB-B. The capacitive voltage transformer (CVT) is represented as a 4400-pF capacitance to ground. The surge arrester (SA) is characterized using a voltage-current curve [26] and includes an inductance of 1 μH/m for a 5-meter cable. The SF6/air bushing (BU) is modeled as a lumped capacitor to ground with a capacitance of 100 pF. The overhead line (OHL) is modeled as a constant distributed parameter system, with a length of 813 meters. The OHL specifications include the following basic dimensions [19]:

- Conductor: ACSR "Grosbeak" (4 x 636 MCM)
- Ground Wire: ACSR "Cochin" (1 x 211.3 MCM)

This detailed configuration facilitates accurate VFTO analysis within the 550 kV GIS environment, providing insights into the transient behavior across the switchgear components.

The simulation diagram of 550 kV GIS is shown in Figure 5.

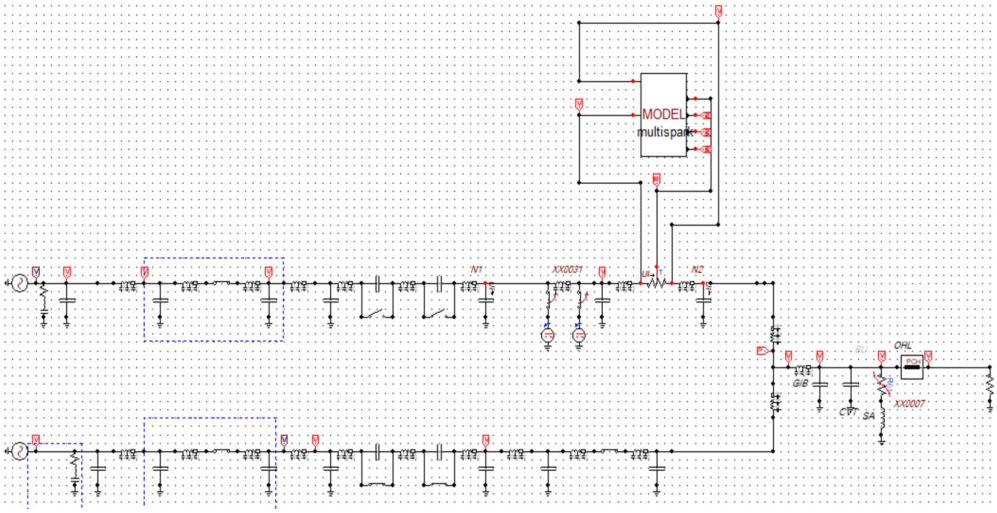

Figure 5. Simulation Diagram of 550kV GIS

4.MULTI-SPARK OPERATION OF DISCONNECTOR SWITCH

The study proposed in this paper projects the opening and closing operation of DS. For VFTO measurement the disconnector switch is supposed to be in closed position. With two different switching velocities, the simulation diagram employing multi spark model for DS operation is shown in Figure 5. The outputs observed for motorised and manual operation are shown in Figure 6.

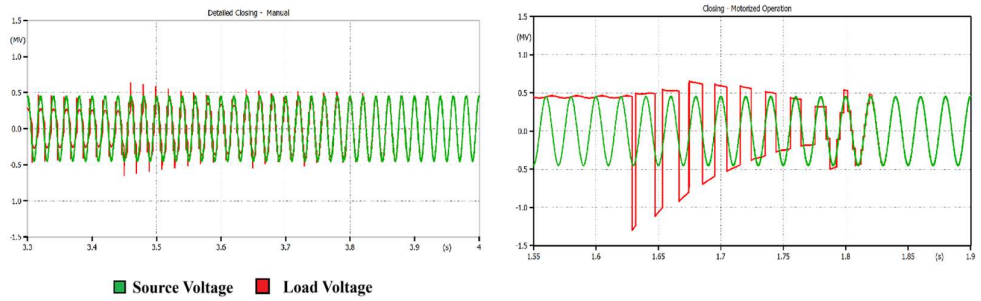

Figure 6. Load and Source Voltage during Closing of DS for Motorized and Manual operation.

4.1. Observations from the closing operation of DS

From the simulated results it can be monitored that number of sparks generated during motorized operation from figure 6 is very less and full closure of DS is achieved at 2.33 seconds which is in agreement with closing time and the instant of first spark ignition. The results from manual operation concludes that full closure of disconnector switch is achieved at 3.93 seconds. The simulated results reveal that with manual operation number of sparks and time of operation increases when compared to motorized closing operation.

4.2. Conclusions from the closing operation of DS

1. Number of sparks increases with decrease in velocity of movement of disconnector switch.
2. Closing duration varies inversely with velocity of switching in DS.
3. It is also deduced that for every 10 times increase in velocity of switching there is substantial improvement in peak overshoot of the load voltage by 10-15%.

5. SIMULATION AND RESULTS

The 550 kV GIS model was simulated and analyzed for key parameters such as rise time, overshoot, and severity factor using EMTP-ATP software. Nodes N_1 and N_2 were analyzed for Very Fast Transient Overvoltages (VFTOs) and residual load through simulations conducted on the 550 kV GIS setup illustrated in Figure 4. Table 1 shows the switching conditions for VFTO and residual measurements.

.

Table 1. States of Switches for Measuring Constraints

CB-B	DS-B	Measurement constraint
OFF	OFF	Residual load
OFF	ON	VFTO

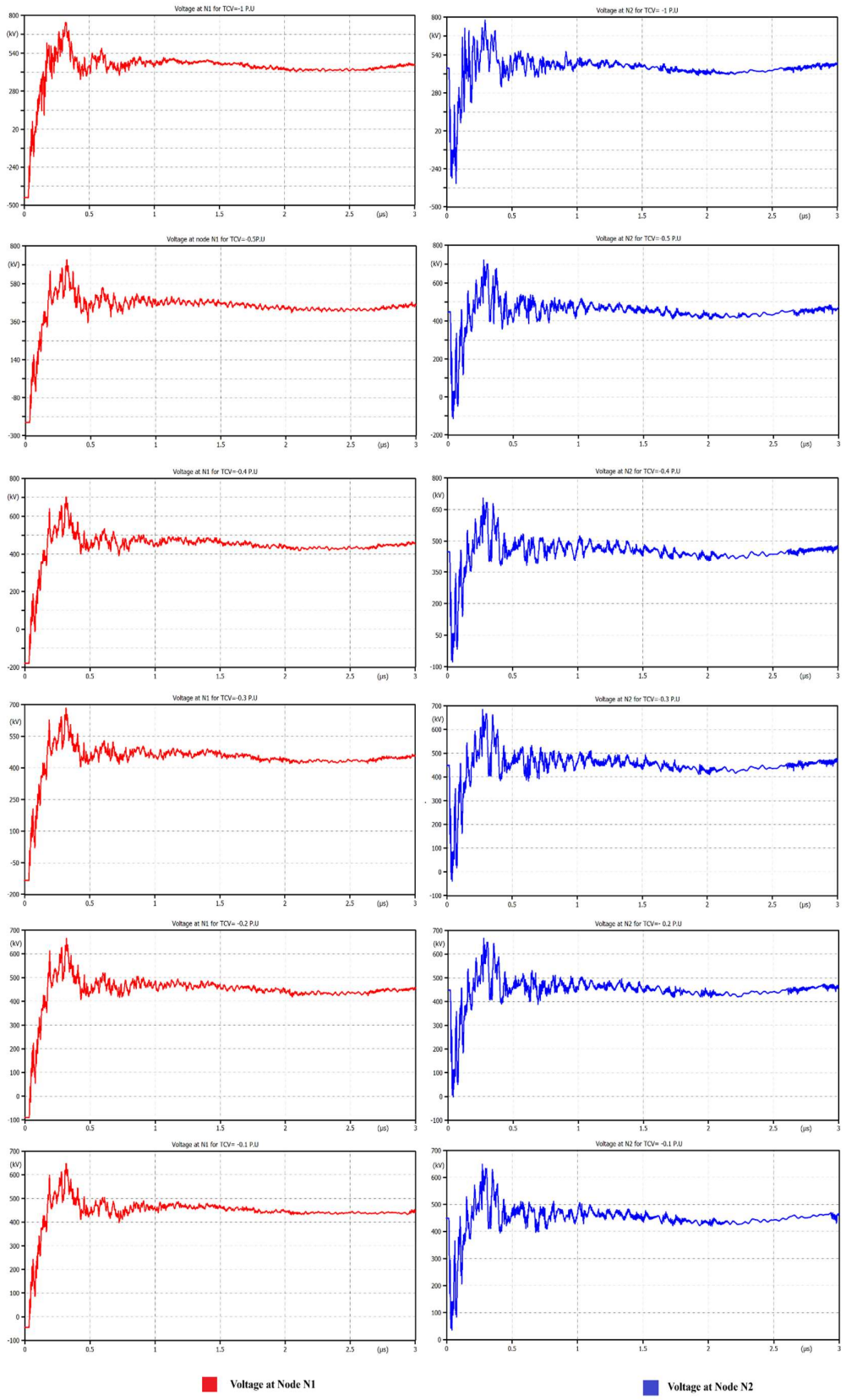

Figure 7. VFTO Monitored at Nodes N_1 and N_2

Observation at Node N_1: Figure 7 displays the VFTO levels monitored at node N_1 under varying trapped charge voltages (TCV) during DS-B's closing operation. The plots corresponding to N_1 demonstrate that higher trapped charge voltages (e.g., -1 p.u in Figure 7) result in larger initial voltage spikes and higher peak VFTO values. As TCV decreases, the observed VFTO magnitude also reduces, indicating a direct relationship between trapped charge levels and VFTO severity at N_1.

Observation at Node N_2: Similarly, Figure 7 illustrates the VFTO levels at node N_2 for the same range of TCVs. The pattern mirrors that of N_1, with higher trapped charges leading to more significant voltage peaks. The plots highlight that VFTOs propagate through the GIS, and node N_2 experiences the residual impacts of VFTO, confirming that even minor trapped charges can propagate substantial transients.

The visual data and corresponding voltage values underline the importance of controlling trapped charges to mitigate VFTO impacts within GIS systems.

6. EVALUATION OF PARAMETERS TO CHARACTERIZE VFTOs

The paper evaluates the VFTOs (Very Fast Transient Overvoltages) generated in a 550 kV GIS system under different Trapped Charge Voltages (TCVs) at critical nodes ($N_1$and N_2). Various response parameters are assessed to determine the VFTO severity [20], including rise time (T_{m1}), peak time (T_{mm}), peak overshoot, maximum voltage, steady-state voltage, and settling voltage. These parameters provide insights into the VFTO behavior and help quantify the system's response during switching operations.

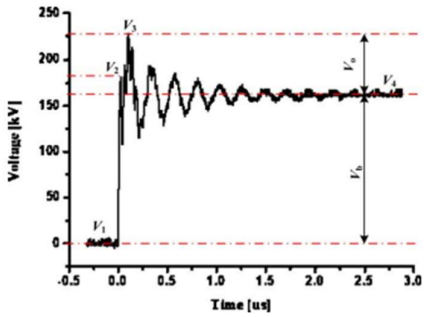

Figure 8. Response Characteristics representing Evaluation Parameters.

The VFTO response characteristics are depicted in Figure 8 [20], illustrating the transient process and various voltage stages. The transitions and parameter definitions observed during the DS switch closing are detailed as follows:

- V_1: Steady-state voltage before transient
- V_2: First maximum after the transient initiation
- V_3: Peak voltage achieved during the transient
- V_4: Steady-state voltage after the transient, generally aligned with the power source voltage

Other key metrics, such as V_o (overshoot voltage), V_b (breakdown voltage), and derived severity indicators K_{m1}, K_{mm}, and K_o, are calculated as follows:

V_o is the voltage overshoot and from the above figure mathematically, $V_o=V_3-V_4$.

V_b is the breakdown voltage which is the difference between two steady state voltages before and after spark and mathematically, $V_b=V_4-V_1$.

After prestrike the steady state voltage V_1 changes to V_4, during this process the voltage undergoes various transitions and are defined as follows:

V_{m1} is the difference between first maximum and steady state voltage before spark. Simply it is the difference between V_2 and V_1, representing the initial rise.

V_{mm} is the difference between peak voltage and steady state voltage before spark or is the difference between V_3 and V_1, capturing the peak voltage excursion
The severity factors—K_{m1}, K_{mm}, and K_o—are calculated as:
where, $K_o=(V_o/V_b)$,
$K_{mm}=(V_{mm}/T_{mm})$,
$K_{m1}=(V_{m1}/T_{m1})$.
These parameters enable the characterization of VFTO severity, where higher values of Ko, K_{mm} and K_{m1} indicate more intense transients.
T_{m1} is the time taken to reach first maximum just after prestrike
T_{mm} is the time taken by the voltage to increase from 10% to 90% of its rated value
All the defined parameters are simulated and tabulated in the below Tables.

6.1. Study of Simulated Results

The simulation results are summarized across TCV values ranging from -1 p.u. to -0.1 p.u. for both N_1 and N_2, as shown in Tables 2 to 3. The following conclusions can be drawn from these tables:

1. TCV Impact on VFTO Parameters: Lower TCVs exhibit reduced peak overshoot, steady-state voltage deviations, and severity factors, indicating that initial trapped charge significantly affects the VFTO characteristics.
2. Comparison of Severity Factors (K_{m1}, K_{mm}, and K_o): The highest overshoot and severity factors are observed at TCV = -1 p.u., gradually decreasing as TCV approaches -0.1 p.u., suggesting a linear relationship between TCV and VFTO severity.

Table 2. Evaluated Parameters obtained by Simulation Results at Node N_1 for TCV= -1.0 P.U and TCV= -0.1P.U

Parameters	TCV= -1p.u	TCV= -0.5p.u	TCV= -0.4p.u	TCV= -0.3p.u	TCV= -0.2p.u	TCV= -0.1p.u
V_1 (kV)	-449.1	-224.5	-179.6	-134.7	-89.1	-44.91
V_2 (kV)	71.4	128.7	148.1	169.6	191.1	212.6
V_3 (kV)	750.5	718.8	700.8	682.8	664.8	646.8
V_4 (kV)	430.1	428.4	425	425.4	424	423.9
$V_o=(V_3-V_4)$	320.4	290.4	275.8	257.4	240.8	222.9
$V_b= (V_4 -V_1)$	879.2	652.9	604.6	560.1	513.1	468.81
T_{m1}(ns)	16	18.9	19	19.4	19.4	20
T_{mm} (ns)	84	94.5	100.4	132.3	132.3	144
$V_{m1}=(V_2-V_1)$ (kV)	520.5	353.2	327.7	304.3	280.2	257.51
$V_{mm}= (V_3-V_1)$ (kV)	1199.6	943.3	880.4	817.5	753.9	691.71
$K_{m1}=(V_{m1}/T_{m1})$ (kV/ns)	32.53	18.69	17.25	15.69	14.44	12.88
$K_{mm}=(V_{mm}/T_{mm})$ (kV/ns)	14.28	9.98	8.77	6.18	5.70	4.80
$K_o=(V_o/V_b)$	0.36	0.44	0.46	0.46	0.47	0.48

In Table 2, the evaluation of parameters for TCV = -1.0 p.u. to TCV = -0.1 p.u. at nodes N_1 gives insights into how VFTO (Very Fast Transient Overvoltage) characteristics change with different transient voltage conditions. Here is a breakdown of key observations for each parameter:

1. Steady-State Voltage (V_1 and V_4): The steady state voltage (V_1) before transient at node N_1 is dependent on the trapped charge voltage for varied TCVs. For an instance at node N_1 for TCV= -1p.u the steady state voltage observed was -449.1 kV, for TCV= -0.5 p.u. Similarly, for variable TCVs between -0.4,-0.3,-0.2,-0.1 p.u the voltage variations were seen proportionally between -179.6 kV to -44.91 kV thereby reflecting the fact that the steady state voltage variations are dependent on surface charge accumulation. Steady state voltage after transient (V_4) across the node N_1 for variable TCV ranging from -1 p.u to -0.1 p.u is monitored to be relatively consistent ranging between 430 kV to 424 kV indicating that the steady-state voltage after the transient (set by the power source) is similar across these conditions.
2. Transient Voltages (V_2 and V_3): The transient voltage V_2 exhibits a marked increase when transitioning from TCV = -1 p.u. (71.4 kV at N_1) to TCV = -0.5 p.u. (128.7 kV at N_1). Likewise, for each TCV variation from -0.4 p.u to -0.1 p.u the voltage shift (V_2) is seen in inverse pattern i.e., 148.1 kV to 212.6 kV This signifies that the first maximum reached by the system is considerably increasing with lower TCVs. The peak voltage V_3 is seen declining as the value of TCVs (-1 p.u to -0.1 p.u) are decreasing i.e., (750.5 kV to 646.8 kV) This decline in V_3 indicates that lower TCV values lead to reduced voltage spikes, which can reduce the severity of VFTOs.
3. Overshoot and Breakdown Voltage (V_o and V_b): The overshoot voltage (V_o) and Breakdown voltage (V_b) is seen following declining pattern at nodes N1 (320.4 kV to 223 kV and 879.2 to 468.81 kV) with decrease in trapped charge voltages (-1 p.u to -0.1 p.u) thereby indicating substantial improvement in system response during transient. These output characteristics signifies decreased overshoot and break down voltage as the trapped charges decreases thereby signifying the impact of trapped charges on the system performance and reliability.
4. Time Parameters (T_{m1} and T_{mm}): The rise timeTm1 and the maximum time Tmm is seen to follow an incline pattern as the value of TCVs decrease from -1 p.u to -0.1 p.u at node N_1. The rise time (TCV=-0.1 p.u) is observed to be increased by 1.25 times rise time monitored at trapped charge of -1 p.u. The time taken to reach maximum voltage is also increased with decrease in the value of TCVs. This trend indicates a significant increase in the T_{m1} and T_{mm} as the TCV becomes less negative. The highest peak time is observed at TCV = -0.1 p.u., demonstrating improved performance at lower TCV values by reduction in damped frequency at the point of measurement.
5. Derived Parameters (V_{m1}, V_{mm}, K_{m1}, K_{mm}, K_o): V_{m1} and V_{mm} both show reductions at lower TCV, signifying a lower voltage deviation from the steady-state before the transient. The severity indicators (K_{m1}, K_{mm}, and K_o) show a general decline with decreasing TCV, at nodes N_1. For instance, K_{m1} decreases from 32.53 at TCV=-1 p.u to 12.88 at TCV= -0.1 p.u, while K_{mm} decreases from 14.28 at TCV= -1p.u to 4.80 at TCV=-0.1 p.u and K_o shows approximately consistent behavior throughout the variations in trapped charges. This reduction in severity indicators with lower TCV values suggests that lower TCVs result in less intense transient effects, potentially mitigating damage to equipment.

Lowering TCV generally decreases the voltage overshoot and peak values, which reduces the severity of VFTO impacts. This is evident from the gradual decrease in values for V_o, V_b, V_{m1}, V_{mm}, and the severity indicators (K_{m1}, K_{mm}, and K_o) as TCV decreases from -1 p.u. to -0.1 p.u., at node N_1. Consequently, this analysis suggests that supressing TCVs [27] could be a strategy to control VFTO intensity and protect electrical components from transient-related stress.

Table 3 presents evaluated parameters obtained from simulation results for TCV values of -1 p.u. and -0.1 p.u., examining node N_2. This analysis highlights key findings and trends regarding voltage behavior and transient characteristics under varying conditions.

1. Steady-State Voltage (V_1 and V_4): The steady state voltages before transient (V_1) at node N_2 is approximately equal to source voltage and is independent of trapped charges. i.e., -1 p.u and -0.5 p.u. The steady-state voltage after transient (V_4) across the node N_2 for variable TCV ranging from -1 p.u to -0.1 p.u is monitored and has been observed to be

relatively uniform, ranging between 414 kV and 408 kV, indicating that the steady-state voltage after transient (set by the power source) is similar across these conditions.

Table 3. Evaluated Parameters obtained by Simulation Results at Node N2 for TCV= -1.0 P.U and TCV= -0.1P.U

Parameters	TCV= -1p.u	TCV= -0.5p.u	TCV= -0.4p.u	TCV= -0.3p.u	TCV= -0.2p.u	TCV= -0.1p.u
V_1 (kV)	449	449.1	449.1	449.1	449.1	449.1
V_2 (kV)	165.5	236.4	250.6	264.8	278.9	293.1
V_3 (kV)	721.9	721.1	702.9	684.8	666.7	648.5
V_4 (kV)	414.7	414.7	410.1	409	408.9	408.9
$V_o=(V_3-V_4)$	307.2	306.4	292.8	275.8	257.8	239.6
$V_b= (V_4 -V_1)$	-34.3	-34.4	-39	-40.1	-40.2	-40.2
T_{m1}(ns)	12.6	14.7	15	16	16	18.1
T_{mm} (ns)	119.7	121.8	122	122.9	124	124.9
$V_{m1}=(V_2-V_1)$ (kV)	-283.5	-212.7	-198.5	-184.3	-170.2	-156
$V_{mm}= (V_3-V_1)$ (kV)	272.9	272	253.8	235.7	217.6	199.4
$K_{m1}=(V_{m1}/T_{m1})$ (kV/ns)	22.50	14.47	13.23	11.52	10.64	8.62
$K_{mm}=(V_{mm}/T_{mm})$ (kV/ns)	2.28	2.23	2.08	1.92	1.75	1.60
$K_o=(V_o/V_b)$	8.96	8.91	7.51	6.88	6.41	5.96

2. Transient Voltages (V_2 and V_3): The first spark after transient V2 demonstrates a significant rise when moving from TCV = -1 p.u. (165.5 kV at N_2) to TCV = -0.1 p.u. (293.1 kV at N_2). This indicates that the system's initial maximum increases significantly with smaller TCVs. The peak voltage V_3 shows a decrease from 721.9 kV to 648.5 kV, indicating similar transient behavior with decreased TCV. The peak voltages V_3 during transient goes on increasing with increase in TCV at both the nodes.

3. Voltage Differences (V_o and V_b): The overshoot voltage Vo is highest at N_2 (307.2 kV) for TCV = -1 p.u., and decreases to 239.6 kV for TCV = -0.1 p.u. This trend reflects a decrease in the peak voltage during transients with decreasing TCV. Breakdown voltage V_b shows substantial values (-34.3 kV for TCV = -1 p.u. at N_2 to - 40.2 kV for TCV = -0.1 p.u. at N_2). Notably, at N_2, as well the overshoot voltage and breakdown voltage follows the same trend as N_1 indicating an increase in system performance as the value of TCV decreases.

4. Time Parameters (T_{m1} and T_{mm}): The parameters like rise time were recorded to increase by 1.43 times rise time of the lowest TCV value indicating non-linear increase in Tm1 at node N_2 whereas peak time simulation results were seen increasing 1.04 times with decrease in TCVs at the point of measurement.

5. Derived Parameters (V_{m1}, V_{mm}, K_{m1}, K_{mm}, K_o): The values for V_{m1} (the difference between V_2 and V_1) highlight significant fluctuations, at N_2, which changes from 283.5 kV (for TCV = -1 p.u.) to 156 kV (for TCV = -0.1 p.u.), indicating a reduction in the voltage differential as TCV decreases. The maximum voltage difference V_{mm} displays a notable decline at N_2 (from 272.9 kV to 199.4 kV), further reinforcing the reduced intensity of transients at lower TCV. The severity indicators K_{m1} and K_{mm} show a downward trend with lower TCV values at point of damage. This indicates reduced peak voltages relative to the time, suggesting a mitigation of transient effects. The ratio Ko (the overshoot to breakdown

ratio) also indicates decreasing intensity with TCV reduction, going from 8.96 to 5.96 at N_2, suggesting a less severe transient behavior with lower TCV.

Table 3 shows that when TCV falls from -1 p.u. to -0.1 p.u., transient and overshoot voltages at N_2 decrease significantly. This lowering improves system stability and reduces the severity of transient occurrences, as shown by the calculated parameters and severity indicators. Overall, maintaining TCV values can be an effective technique for limiting transient reactions in power systems, thereby increasing the reliability and longevity of Gas Insulated switchgear.

7. GRAPHICAL REPRESENTATION OF DERIVED PARAMETERS TO ANALYSE VFTO SEVERITY

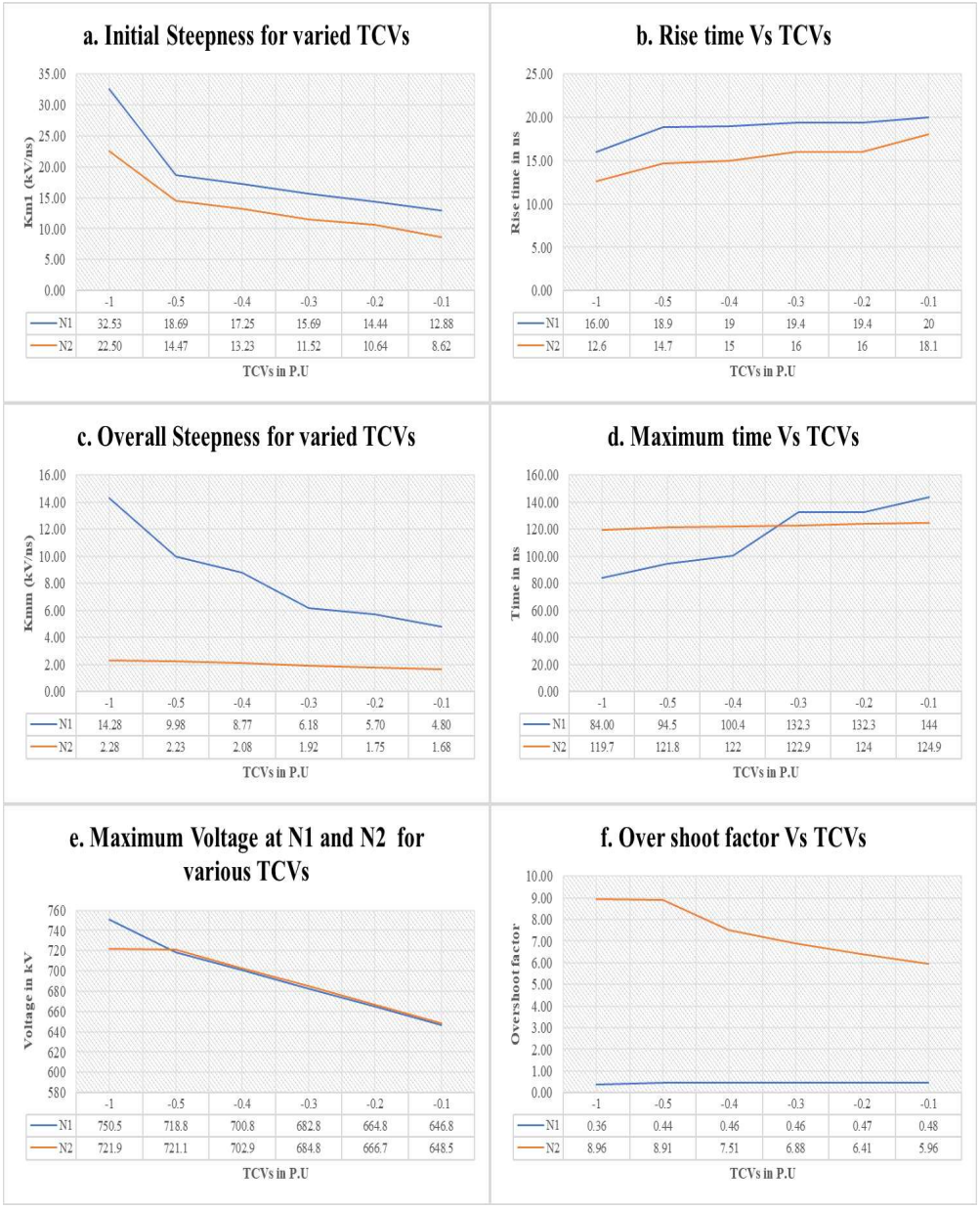

Figure 9. Plotted Data to Evaluate Severity Index for VFTO

Figure 9 provides a comprehensive graphical investigation on all the severity indexes that are responsible to enhance VFTO. Figure. 9 (a) depicts the variation of initial steepness with respect to variable TCVs. Figure 9 (b) presents the deviation of rise time to wide range of TCVs from -1p.u to -0.1 p.u. Figure 9 (c) & (d) represents the variation of TCVs corresponding to its overall steepness and maximum time taken by the response to reach its peak after transient. Figure 9 (e) & (f) are the variation in trapped charges to peak voltage and overshoot factor respectively.

7.1. Conclusions from Graphical Data:

a. Initial steepness and Rise Time: These are non-linearly related to each other i.e., with the increase in rise time the steepness of the voltage characteristics is reduced. This suggests that as the time taken by the characteristics to reach at least 10% of the response is delayed, the steepness of the curve is reduced thereby lowering the severity of VFTO. Figure 9 (a) displays the decrease in initial steepness as the trapped charges varies from -1 p.u to -0.1 p.u at both N_1 and N_2 consequently the rise time is seen increasing as we move on from left to right on the horizontal axis. Figure 9 (a) & (b) both illuminates that both initial steepness and rise time are higher at node N_1.

b. Over all steepness and Maximum time: These parameters also follow the same trend as Figure 9 (a) & (b) since overall steepness and maximum time are inversely related to each other. Pictorial analysis reveals that broader change in both the parameters at N_1 is observed whereas at N_2 the change is very moderate. Also, node N_1 experiences the highest values of overall steepness and maximum time compared to N_2.

c. Maximum Voltage and Over shoot Factor: Maximum voltage or peak value of the voltage is directly related to over shoot factor. From Figure 9 (e) it can be monitored that as the value of TCV is decreasing the peak voltage value also decreases. Also, the maximum voltage is observed at node N_1. From Figure 9 (f) the overshoot factor is seen following direct relationship with respect to peak voltage at node N_2 and approximately constant throughout the variation in TCVs at node N_1.

These insights provide a comprehensive comparison of derived parameters like rise time (T_{m1}), peak time (T_{mm}), over shoot factor (K_o), Initial and overall steepness (K_{m1} & K_{mm}) for various TCV (Trapped Charged Voltage) values across two nodes (N_1 and N_2). This analysis highlights the temporal behavior of the system's voltage response under different TCV conditions thereby making it crucial to understand these dynamics for best optimization of trapped charges [27] in order to control these very fast transients over voltages which is problem of concern while working with EHV/UHV transmission system.

8. STRATEGIES FOR SUPRESSING SURFACE CHARGE ACCUMULATION

Surface charge accumulation over the insulator surface in gas insulated switchgear is very vital since it deteriorates the insulation level thereby impacting the transmission capabilities. Previous literature suggests many works in developing new composite nano dielectric material in order to supress these charges since they become a serious concern while working with EHV/UHV transmission levels. Few of techniques involve

- Doping of epoxy resin by MXene, a two-dimensional nanomaterial to reduce surface charge buildup [27].
- Surface fluorination of Al_2O_3- filled epoxy resin disc insulators [28].
- Plasma treatment of epoxy resin insulators deposited by SiO_X thin films [29].
- Enhancing the moisture content on the surface of fluorinated epoxy resin insulator [30] in order to enhance the dielectric strength of the insulator.

Therefore, abundant research is in progress to suppress these surface charges by expansion of various material composition. Hence by controlling and managing trapped charges the severity of VFTO is reduced ensuring GIS insulation reliability and operational resilience.

9. CONCLUSION

The study offers a comprehensive evaluation of Very Fast Transient Overvoltages (VFTOs) in a 550 kV Gas-Insulated Switchgear (GIS) system, focusing on the significant impact of Trapped Charge Voltage (TCV) during disconnector switch operations. By developing multi-spark disconnector switch model using EMTP-ATP software, this work quantitatively demonstrates that increased TCV levels lead to heightened VFTO magnitudes, faster peak times, and higher overshoot factors, all of which intensify stress on GIS insulation.

Quantitative analysis in this study indicates that TCV variations can amplify VFTO magnitudes by up to 15%, with overshoot factors and peak response times reflecting similar increases under high TCV conditions. This research focusses on model's ability to accurately simulate TCV-induced VFTO severity provides an effective tool for assessing GIS insulation needs and operational resilience. Additionally, the observed inverse relationship between trapped charge capacitance and VFTO magnitude offers a promising avenue for mitigation: controlling TCV parameters could serve as a proactive strategy to limit VFTO effects, thereby enhancing GIS system stability. The contributions of this study extend beyond simulation validation; they provide actionable insights for designing GIS systems with enhanced insulation resilience, operational protocols to manage TCV levels effectively, and the foundation for future VFTO mitigation strategies. By bridging a key gap in quantitative TCV analysis, this research establishes a robust framework that can be adapted to varied GIS configurations and voltage levels. Future research directions may explore alternative switching mechanisms, advanced TCV management techniques with better nanomaterial composition and cross-compatibility with other high-voltage systems, further factors while designing an industrial HVDC GIL insulator like flashover performance, partial discharge, and leakage current.

REFERENCES

[1] D'Souza, Merwyn, Ravi S. Dhara, and Rene C. Bouyer. "Modularization of high voltage gas insulated substations." IEEE Transactions on Industry Applications 56, no. 5 ***(2020)****: 4662-4669.*

[2] Reddy, Sheri Abhishek, and M. Sailaja Kumari. "A review of switching overvoltage modeling in UHV AC transmission lines." Electric Power Systems Research 236 ***(2024)****: 110902.*

[3] Nagarsheth, Raj, and Sushant Singh. "Study of gas insulated substation and its comparison with air insulated substation." International Journal of Electrical Power & Energy Systems 55 ***(2014)****: 481-485.*

[4] Scherer, Harold N., and Gregory S. Vassell. "Transmission of electric power at ultra-high voltages: current status and future prospects." Proceedings of the IEEE 73, no. 8 ***(1985)****: 1252-1278.*

[5] Insulation co-ordination - Computational guide to insulation co-ordination and modelling of electrical networks ***IEC TR 60071-4:2004.***

[6] Wu, Yongji, Wei Yan, Hongtian Chen, Wu Zhang, and Hao Ma. "Research on interferences of VFTO to irregular distributions of secondary side cables." IEEE Transactions on Power Delivery 38, no. 1 ***(2022)****.*

[7] Maziar Babaei, Sherif Abdelwahed, Mehdi Babaei, "Transient Ground Potential Rise in Gas Insulated Substations and Analysis of Effective Factors", Proceedings of the ASME 2015 Power Conference POWER, ***(2015)*** *June 28- July 2, San Diego, California.*

[8] M. A. Abd-Allah, A. Said, and Ebrahim A. Badran, "High-Frequency Spectrum Analysis of VFTO Generated inside Gas Insulated Substation", World Academy of Science, Engineering and Technology Vol:79 ***(2013)*** *July 22.*

[9] Mariusz Stosur, Marcin Szewczyk, Wojciech Piasecki, Marek Florkowski, Marek Fulczyk, "GIS disconnector switching operation – VFTO study", Modern Electric Power Systems (MEPS), ***(2010)*** *Proceedings of the International Symposium: Wroclaw, Poland.*

[10] Caiquan Wen, Zheng Yang, Yitao Lu, Yongfeng Huang, Hanliang Lin, Zhiyuan Zhang, Taiyu Chen, and Yingnan Liu , "Study on Very Fast Transient Overvoltage Characteristics of Gas-Insulated Switchgear Substation Based on Hybrid Reactive Power Compensation", Hindawi Mathematical Problems in Engineering Volume ***(2022).***

[11] Reem A Almenweer, Yixin Su and Xixiu Wu, "Comparison between suppressing approaches of very fast transient over voltages in gas insulated substation", IOP Conf. Series: Journal of Physics: Conf. Series 1303 ***(2019).***

[12] J. Ozawa, T. Yamagiwa, M. Hosokawa, S. Takeuchi, H. Kozawa, "Suppression of Fast Transient over voltage during Gas Disconnector Switching in GIS", IEEE Transactions on Power Delivery, Vol. PWRD-1, No. 4, ***(1986)*** *October.*

[13] Hengtian Wu, Weiran Fang, "Influences on very fast transients induced on secondary cables of GIS substation", Journal of Physics: Conference Series 1846 ***(2021).***

[14] Lei Zhao, Ruming Feng, Chuanqiang Che, Tianyu Liu, Jiali Chong, Huijun Wang, Jun Zhao, "Numerical Simulation Calculation Analysis of Very Fast Transient Overvoltage Arcing", IEEE 2nd China International Youth Conference on Electrical Engineering (CIYCEE), ***(2021).***

[15] M. SZEWCZYK, "Multi-spark modelling of very fast transient over voltages for the purposes of developing HV and UHV gas-insulated switchgear and of conducting insulation co-ordination studies", Bulletin of The Polish Academy of Sciences Technical Sciences, Vol. 65 ***(2017).***

[16] Mariusz Stosur, Marcin Szewczyk, Wojciech Piasecki, Marek Florkowski, Marek Fulczyk, "GIS disconnector switching operation – VFTO study", ABB Corporate Research Center in Krakow Starowislna 13A, 31-038 Krakow, ***(2010)*** *Poland.*

[17] S.A. Boggs, F.Y. Chu and N. Fujimoto, "Disconnect Switch Induced Transients and Trapped Charge in Gas-Insulated Substations", IEEE Transactions on Power Apparatus and Systems, Vol. PAS-101, No. 10 ***(1982)****, October.*

[18] Maziar Babaei, Maziar Babaei, Ghasem Nourirad, "Analysis of Influential Factors in Determining Very Fast Transient Over voltages of GIS", 2014 IEEE 8th International Power Engineering and Optimization Conference (PEOCO2014), Langkawi, The Jewel of Kedah, Malaysia. ***(2014)*** *March 24-25.*

[19] D.C. Moreira, M.V.A. Nunes, D.D.C. Moreira, D.K.D. Costa, "Analysis of VFTO during the failure of a 550-kV gas-insulated substation", Electric Power Systems Research 189 ***(2020)*** *106825.*

[20] Yonggang Guan, Gongchang Yue, Weijiang Chen, Zhibing Li, Weidong Liu, "Experimental Research on Suppressing VFTO in GIS by Magnetic Rings", IEEE Transactions on Power Delivery, Vol. 28, No.4, ***(2013)****, October.*

[21] Szewczyk, Marcin, Maciej Kuniewski, Wojciech Piasecki, Marek Florkowski, and Ueli Straumann. "Determination of breakdown voltage characteristics of 1'100 kV disconnector for modeling of VFTO in gas-insulated switchgear." IEEE Transactions on Power Delivery 31, no. 5 ***(2015)***

[22] Salah, Mohamed, Ebrahim A. Badran, and Mansour H. Abdelrahman. "The Transformer Modelling for VFTOs Calculation-A Comprehensive Review Mohamed Salah." Mansoura Engineering Journal 49, no. 5 ***(2024).***

[23] Sun, Qiang, Ziwei Zhang, Wensheng Gao, Dengwei Ding, Yanpeng Ge, and Jiaqi Qu. "Accurate and Rapid 3D Full-Maxwell Simulations of Very Fast Transients in GIS Based on a Novel Busbar Voltage Setting Method." IEEE Transactions on Power Delivery ***(2024).***

[24] Zhang, Lu, Sen Wang, Lei Sun, Chen Mao, Lu Pu, and Qiaogen Zhang. "Prediction model of voltage–time characteristics for SF6 long gap under VFTO and lightning impulse voltage." IET Generation, Transmission & Distribution 12, no. 4 ***(2018).***

[25] Chu, Penghao, Bin Wang, Huiguang Zhao, Mingji Shang, and Wenbin Zhao. "Simulation and Experimental Study of VFTO Transient Signals Generated by Considering GIS Disconnect Switch Operation." In Frontier Academic Forum of Electrical Engineering, pp. 959-971. Singapore: Springer Nature Singapore, ***(2022)****.*

[26] J.A. Martinez-Velasco, Transient Analysis of Power Systems: Solution Techniques, Tools and Applications, Wiley, IEEE Press, Chichester, United Kingdom, ***(2015)****.*

*[27] Tianyu Wang, Guixin Zhang, Dayu Li, Yicen Hou and Boya Zhang, "MXene-doped Epoxy Resin to Suppress Surface Charge Accumulation on Insulators in a DC Gas-insulated System", IEEE Transactions on Dielectrics and Electrical Insulation Vol. 27, No. 3; (****2020),*** *October.*

[28] B. Zhang et al, "Suppression of surface charge accumulation on Al2O3 filled epoxy resin insulator under dc voltage by direct fluorination," AIP Adv., vol. 5, no. 12, pp. 127207, ***(2015).***

*[29] T. Shao et al, "Correlation between surface charge and DC surface flashover of plasma treated epoxy resin," IEEE Trans. Dielectr. Electr. Insul., vol. 25, no. 4, pp. 1267–1274, (****2018)****.*

[30] A. Mohamad, G. Chen, Y. Zhang, and Z. An, "Moisture effect on surface fluorinated epoxy resin for high-voltage DC applications," IEEE Trans. Dielectr. Electr. Insul., vol. 23, no. 2, pp. 1148–1155, ***(2016).***